Optical Metasurface Based on the Resonant Scattering in Electronic Transitions

Ming Zhou,[†] Jingfeng Liu,[†,‡] Mikhail A. Kats,[†,§] and Zongfu Yu[*,†,§]

[†]Department of Electrical and Computer Engineering and [§]Department of Material Science and Engineering, University of Wisconsin−Madison, Madison, Wisconsin 53706, United States
[‡]College of Electronic Engineering, South China Agricultural University, Guangzhou 510642, China

S Supporting Information

ABSTRACT: Metasurfaces are an emerging platform for manipulating light on a two-dimensional plane. Existing metasurfaces comprise arrays of optical resonators such as plasmonic antennas or high-index nanorods. In this article, we describe a new approach to realize metasurfaces based on the resonant scattering in electronic transitions, such as in two-level systems (TLSs). These metasurfaces can reproduce all of the major results in conventional metasurfaces. In addition, since TLSs can be easily tunable and are orders of magnitude smaller than optical resonators, TLS metasurfaces can realize functions that are difficult to achieve with optical resonators.
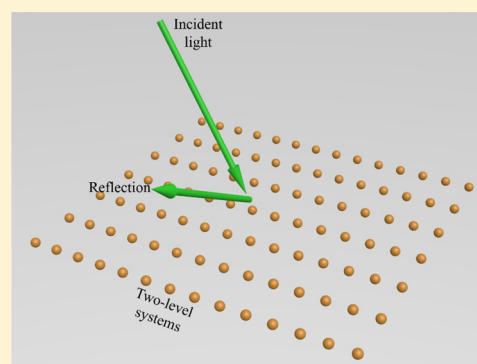
KEYWORDS: metasurface, two-level system, resonant scattering, spontaneous emission

Conventional metasurfaces have seen explosive development in the past few years.[1−14] These optically functionalized surfaces offer completely new ways to control light and have enabled new phenomena such as anomalous reflection,[1] extreme nonlinearity,[7] and the spin Hall effect,[6] as well as applications such as flat lenses,[3] cloaking,[11,12] and generation of vortex beams.[14]

Figure 1a illustrates the operation principle of conventional metasurfaces.[15,16] A subwavelength optical resonator, for example a nanorod made from a high-index material,[17] imparts a phase onto the incident plane wave.[1] The phase of the scattered light ranges from 0 to π and is determined by the relative frequency detuning between the incident light and the resonance. Rods with different radii have different resonant frequencies, thereby creating different scattering phases (Figure 1b).

Optical phase can also be acquired through the scattering process in electronic transition. Here, we consider a generic model of two-level systems (TLSs). A TLS can capture the energy of a single photon and store it in the excited quantum state for a brief moment, during which a phase is accumulated. The probability amplitude of a single photon scattered by a TLS is calculated and shown in the inset of Figure 1c. The scattering phase, which measures the phase difference between the incoming and outgoing light at the location of the TLS, ranges from 0 to π depending on the relative energy detuning, $\Delta E/\Gamma = (E - E_{ph})/\Gamma$, where E is the transition energy of the TLS, Γ is the energy bandwidth, and E_{ph} is the energy of the incident photon. Figure 1c shows the relation between the

scattering phase and $\Delta E/\Gamma$, which resembles that of optical resonators (Figure 1a). An array of TLSs with varying transition energies can create different scattering phases, as shown in Figure 1d. Similar to the optical resonator array (Figure 1b), the TLS array can tilt the phase front and steer the directions of reflection and refraction. TLSs can be found in atoms and molecules. Many solid-state implementations are also rapidly emerging, such as quantum dots,[18] nitrogen-vacancy centers in diamond,[19] and Josephson junctions.[20]

TLS metasurfaces can realize unique features that are extremely challenging for their conventional counterparts. First, TLS metasurfaces are naturally reconfigurable, even in the visible wavelength range. The energy levels of TLSs can be rapidly tuned using laser illumination[21] or external electric[22] or magnetic fields.[23] In contrast, existing reconfigurable metasurfaces rely on incorporating a material with a tunable refractive index into the optical resonators, but achieving a large tuning range has remained a challenge, especially at visible frequencies.[24−27] Second, the scattering elements in TLS metasurfaces can be extremely low loss, with quantum efficiencies in certain quantum dots reaching nearly 100%.[28] Furthermore, their scattering efficiency, measured by the ratio between the optical and physical cross sections, can be extremely large (~10 000),[29] 3−4 orders of magnitude larger than that of optical resonators.[30] The extremely compact size of individual elements, which is unattainable in either dielectric or
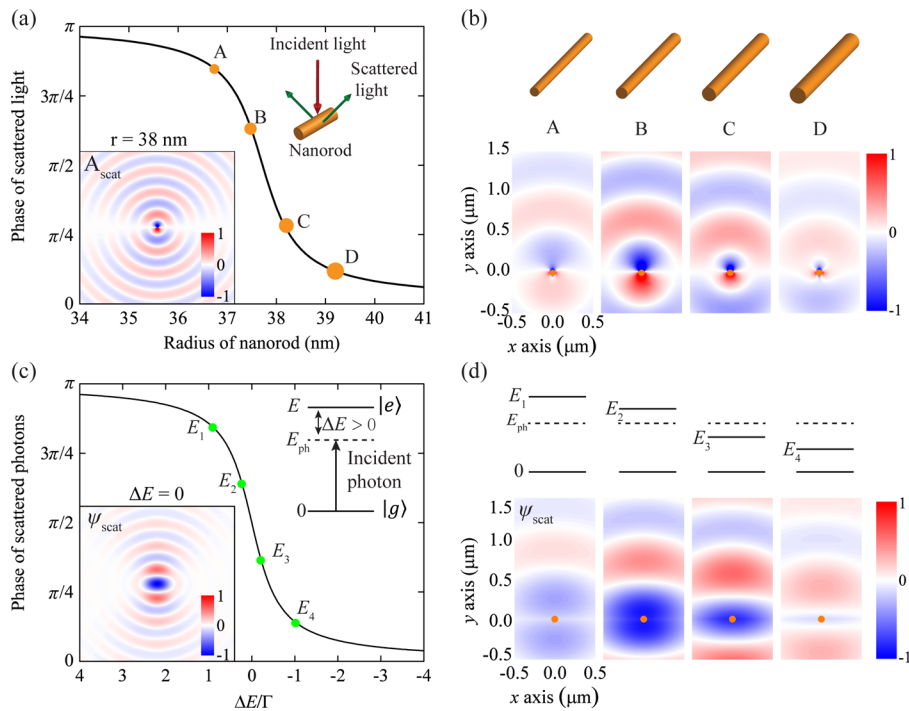
Figure 1. Working principle of conventional and TLS metasurfaces. (a) Scattering phase created by nanorods of different radii. We assume the phase of the incident light at the location of the nanorods is zero. The index of the nanorod is 10, and the incident wavelength is 1 μm. The nanorod is along the z-axis, and the incident electric field is along the x-axis. The resonant scattering is caused by the fundamental magnetic dipole mode of the nanorod. As the radius of the nanorod increases, the resonant frequency decreases, and the phase of scattered light varies from π to 0. The lower inset shows a typical normalized scattering field calculated from a full-wave simulation. (b) A tilted phase front can be synthesized from light scattered by an array of nanorods with different radii. All fields in (a) and (b) are normalized by the magnitude of incident light. (c) Scattering phase created by TLSs of different transition energies. We also assume the phase of the incident photon at the location of the TLSs is zero, and the polarization is also along the x-axis. The energy detuning is normalized by the TLS line width Γ. The upper inset shows the energy levels. The lower inset shows the wave function of scattered single photons Ψ_{scat} (see Section 1, Supporting Information). (d) A tilted phase front can be synthesized from photons scattered by TLSs with different transition frequencies. All fields in (c) and (d) are normalized by the magnitude of the incident photon.

metallic optical resonators, is particularly attractive for synthesizing metasurfaces for advanced functionalities such as multiband operation.[31]

In this article, we theoretically demonstrate examples of TLS metasurfaces that can realize tunable single-photon steering and beaming of spontaneous emission. The properties of a TLS metasurface containing M TLSs are directly studied based on the solution to the Hamiltonian:[29]

$$H = H_0 + H_I \tag{1}$$

The first term is the free Hamiltonian $H_0 = \sum_{m=1}^{M} \hbar \omega_m \sigma_m^\dagger \sigma_m + \sum_{\mathbf{k}} \hbar \omega_{\mathbf{k}} c_{\mathbf{k}}^\dagger c_{\mathbf{k}}$, including all constituent TLSs and the free space photons. Here $\hbar$ is the reduced Planck constant and $\sigma_m^\dagger$ (σ_m) is the raising (lowering) operator of the mth TLS, which has a transition frequency of ω_m. The creation (annihilation) operator for photons with an angular frequency $\omega_{\mathbf{k}}$ is $c_{\mathbf{k}}^\dagger (c_{\mathbf{k}})$, with $\mathbf{k}$ being the momentum of photons. The second term $H_I = i\hbar \sum_{m=1}^{M} \sum_{\mathbf{k}} g_{\mathbf{k},m} (c_{\mathbf{k}}^\dagger e^{-i\mathbf{k}\cdot\mathbf{r}_m} \sigma_m + c_{\mathbf{k}} e^{i\mathbf{k}\cdot\mathbf{r}_m} \sigma_m^\dagger)$ describes the interaction between the TLSs and photons under the dipole and rotating-wave approximations.[29] The position of the mth TLS is $\mathbf{r}_m$, and the coupling strength between the TLS and photons is $g_{\mathbf{k},m}$. The above Hamiltonian can be solved by semiclassical approaches.[32] Here, we use a scattering theory developed in refs 33 and 34, which uses Fock states to describe the incident light and directly calculate the

eigenstates of the Hamiltonian in the free space. The details are available in Section 1 of the Supporting Information.

■ RESULTS AND DISCUSSION

Reconfigurable TLS Metasurface. A metasurface has to create different scattering phases at different locations. Most conventional metasurfaces achieve the phase variation by using optical resonators with different resonant frequencies, which can be done easily by using resonators of different sizes. In contrast, it would be difficult to find TLSs with their natural energy level continuously varying in a controlled way. To overcome this difficulty, we exploit dressed quantum states in three-level systems, for example, ^{87}Rb atoms.[35] The transition energy to a dressed state can be easily tuned through laser illumination. A spatially structured illumination can create a spatially varying scattering phase. More importantly, since the resonant transition is controlled by external input, these metasurfaces do not require precise control of the locations of TLSs and can be rapidly reconfigured.

The energy level diagram of an ideal three-level Λ-type system is shown in Figure 2a. When illuminated by a control laser at the same wavelength with the transition between the states $|2\rangle$ and $|3\rangle$, the two states are resonantly coupled, creating two dressed states, $|a\rangle = (1/\sqrt{2}(|2\rangle + |3\rangle))$ and $|b\rangle = (1/\sqrt{2})(|2\rangle - |3\rangle))$. The energy levels of the two dressed states are separated by a Rabi frequency $\Omega_c = d_{23}|A_c|/\hbar$, where d_{23} is the transition dipole moment between states $|2\rangle$ and $|3\rangle$ and $|$
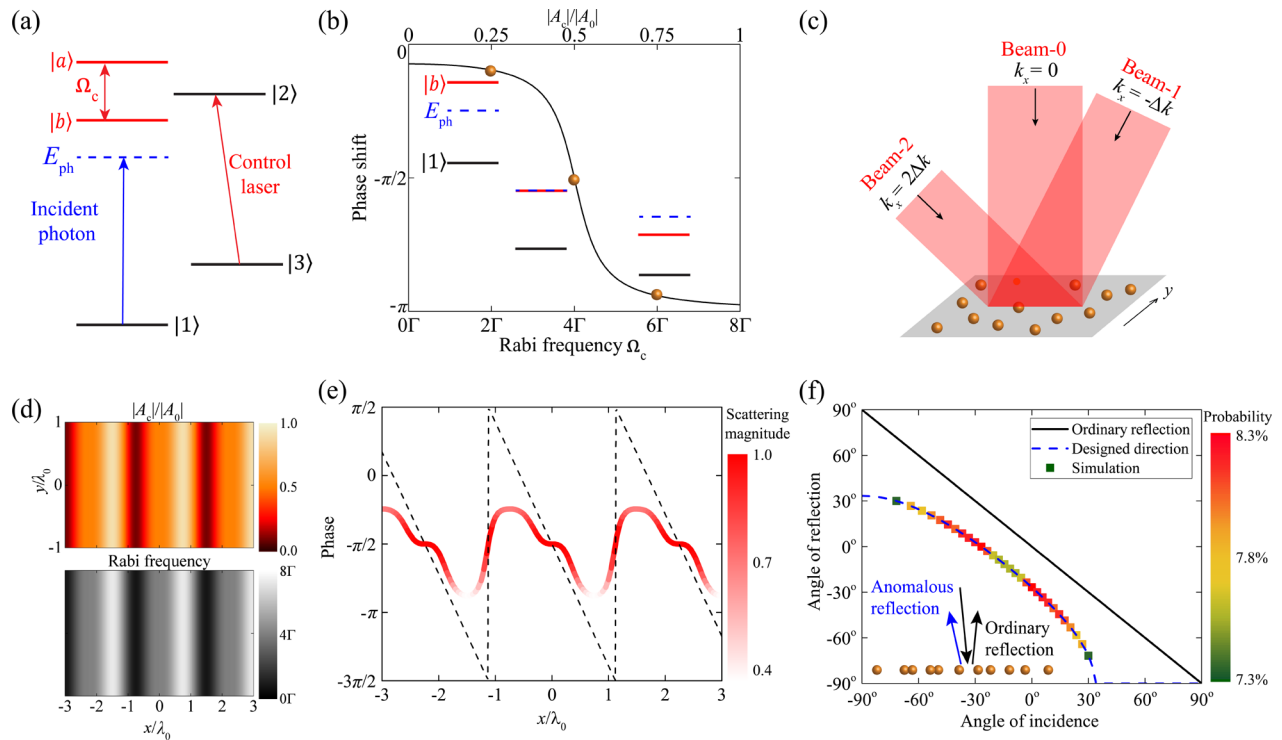
Figure 2. Reconfigurable TLS metasurface made from ideal three-level systems. (a) Energy diagram of three-level systems. When the states $|2\rangle$ and $|3\rangle$ are coupled by the control laser, two dressed states, $|a\rangle$ and $|b\rangle$, are created. The transition between the ground state $|1\rangle$ and the lower dressed state $|b\rangle$ serves as a tunable TLS to be used in a TLS metasurface. (b) Scattering phase for an incident photon with fixed energy as indicated by the blue dashed line. The amplitude of control laser A_c is normalized by A_0, which corresponds to a Rabi frequency of 2Γ, and Γ is the energy bandwidth between states $|1\rangle$ and $|2\rangle$. As the amplitude of control laser and the Rabi frequency changes, the phase spans a range of approximately π. (c) Schematic of the metasurface with three-level systems randomly positioned on the $x-y$ plane. The interference of three control beams creates a spatial profile that tunes the Rabi frequencies at different locations. (d) Spatial profile of normalized electric field of the control beams (upper panel) and the Rabi frequency (lower panel). (e) Spatial profile of the scattering phase. The scattering amplitude is encoded by the weight of the red curve. The black dashed line indicates the ideal phase gradient to impart a phase gradient of Δk to the incident photons. (f) Incident photons are steered to the designed direction (blue dashed line). Simulation results (square markers) are calculated from the scattering theory (see Section 1, Supporting Information). The inset shows a schematic of the directions of the incident, ordinary reflection, and beam steering.

$A_c|$ is the magnitude of the electric field of the control laser. A new TLS is formed between $|1\rangle$ and the dressed state $|b\rangle$. Most importantly, its transition energy $E = E_2 - E_1 - \hbar\Omega_c/2$ is dynamically tunable because Ω_c is linearly proportional to the amplitude of the control laser. Using a control laser with spatially varying illumination, we can create arrays of spatially varying TLSs.

Figure 2b shows the scattering phase of a single photon scattered by the three-level system. The photon energy E_{ph} is chosen to be close to, but detuned from, the transition energy between $|1\rangle$ and $|2\rangle$ (blue dashed line in Figure 2a). As an example, we set $E_{ph} = E_2 - E_1 - 2\Gamma$. When the control laser is off, the scattering phase is nearly zero since its frequency is far away from any resonance. As we turn on the control laser and increase its intensity, the Rabi frequency increases and $|2\rangle$ splits into two states. As the energy of the lower dressed state $|b\rangle$ decreases and approaches the resonant energy level $E_1 + E_{ph}$, the scattering phase decreases (Figure 2b). When $|b\rangle$ sweeps across the resonant level, the phase varies over a range of approximately π.

Now we can design a reconfigurable TLS metasurface using three-level systems as building blocks. The scattering elements are *randomly* placed on a plane. The average density of scattering elements is 4 elements per area of λ_0^2, where λ_0 is the transition wavelength between states $|1\rangle$ and $|2\rangle$. The metasurface is designed to have a spatial phase gradient $\Delta k =$

$\Delta\phi/\Delta x$ along the $\hat{x}$-axis, which steers the incident single photons away from the ordinary reflection direction (Figure 2f). To create this phase gradient, we use three beams from the same control laser to generate structured illumination. Figure 2c shows the directions of these beams. Their wave vectors in the x direction are $k_x = 0$, $-\Delta k$, and $2\Delta k$, respectively. The resulting interference pattern is plotted in the upper panel in Figure 2d (more details in Section 2, Supporting Information). The Rabi frequency (lower panel) follows the same pattern. Figure 2e shows the corresponding scattering phase at different spatial locations. A π phase range is realized. The scattering amplitude is encoded by the weight of the red line in Figure 2e and is designed to maximize the scattering strength in the region where it approximates a linear phase gradient.

We solve the full Hamiltonian of the metasurface, which contains over 1600 scattering elements within an area of $20\lambda_0$ by $20\lambda_0$. The solution takes into account the collective interactions, such as the superradiance effect.[36] It is necessary to perform such a full simulation in order to confirm the designs based on the scattering phase of individual elements. Specifically, we consider a single photon incident from an angle θ_i. The ordinary reflection direction is shown by the black solid line in Figure 2f with $\theta_r = -\theta_i$. The metasurface is designed to steer the reflection to a different direction[1] with $\theta'_r = \sin^{-1}(\Delta k/k_0 - \sin\theta_i)$. Blue dashed line in Figure 2f shows the designed direction for the anomalous reflection with a phase gradient of
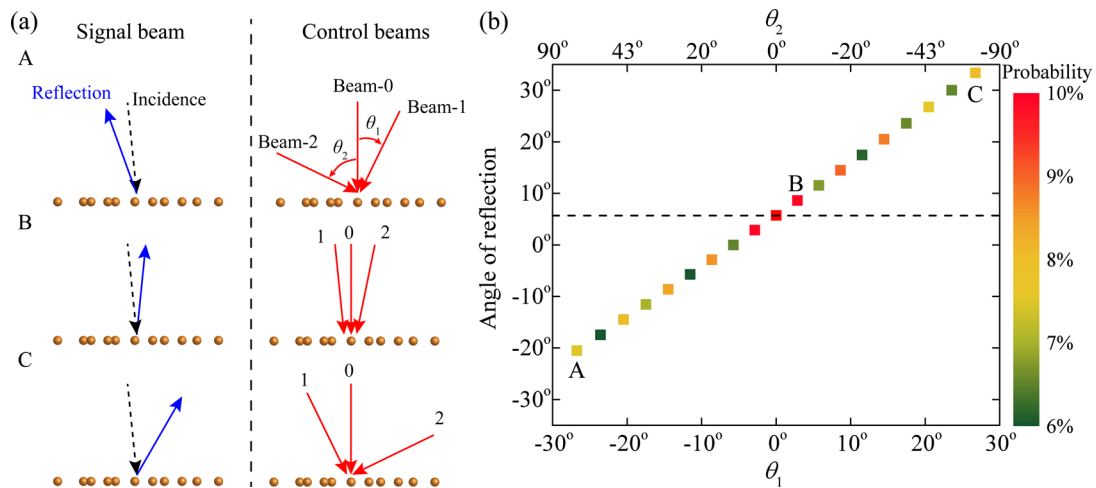
Figure 3. Dynamic beam steering of single photons by a reconfigurable TLS metasurface. (a) The signal beam (blue arrows in the left panels) is steered to different directions depending on the s indicated by the dashed line. Square markers represent the angles and the efficiency of the steered beam. Results are calculated from the quantum scattering theory (see Section 1, Supporting Information).
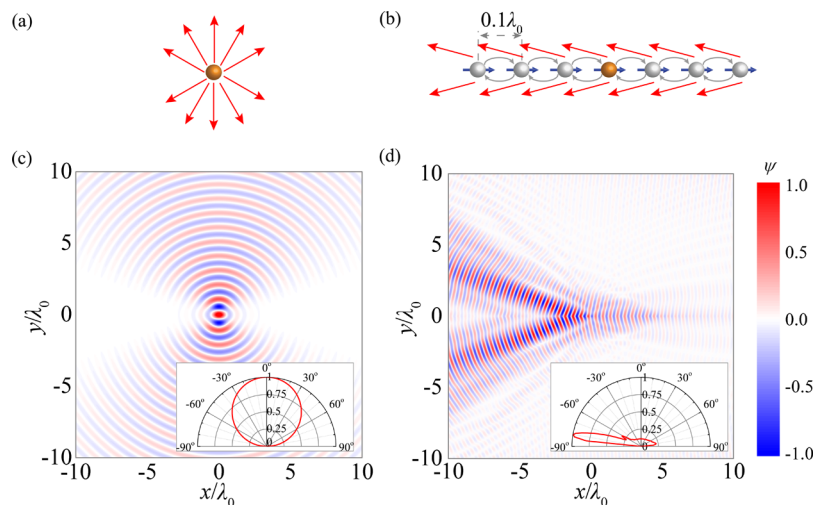

Figure 4. Spontaneous emission of single photons with enhanced spatial coherence. (a) Single excited TLS in free space. (b) Single excited TLS (golden sphere) in a metasurface. All the other TLSs (gray spheres) are initially in the ground state. The total length of the metasurface is $40\lambda_0$, with an inter-TLS spacing of $0.1\lambda_0$, where λ_0 is the resonant wavelength of the excited TLS. All TLSs have the same lifetime τ. (c and d) Snapshots of the real part of wave function at time $t = 3\tau$ for a single excited TLS in free space (c) and within the metasurface (d). The insets show the angular distributions of the total spontaneous emission integrated over all time.

$\Delta k = -0.9\pi/\lambda_0$. We specifically calculate the probabilities of scattered single photons moving in each direction. The results from calculation are shown by square markers. Two major reflections—the ordinary and anomalous reflection—are observed, which agree with the predication well. The probability of incident photons that are steered to the anomalous reflection, which is between 7.3% and 8.3% (Figure 2f), is indicated by the color of the markers. The random positioning of the elements also leads to weak diffusive reflections, which is too small to be observed.

Next, we demonstrate the dynamic steering of single photons by tuning the directions of the control beams as shown in Figure 3a. The phase gradient Δk is tuned from $-0.9\pi/\lambda_0$ to $0.9\pi/\lambda_0$, resulting in different steering directions, as shown by the blue arrows in Figure 3a. To realize this tuning range, beam 0 is always incident from the normal direction. The incident angle of the first beam (θ_1) changes from $-27°$ to $27°$ counterclockwise, while that of the second beam (θ_2) changes from $64°$ to $-64°$ clockwise. Figure 3b shows the results when

the reflected single photons are dynamically steered from $-20°$ to $33°$ as the control beams vary. The color of the markers in Figure 3b indicate the probability of the scattered single photon in the anomalous direction. This steering efficiency remains about the same for different steering angles.

The proposed metasurfaces are within current experimental capabilities. Structured illumination on rubidium atoms has been demonstrated for diffraction gratings.[37] Site-controlled arrays of quantum dots are also a promising approach to realize the reconfigurable metasurface.[38] Optical lattices of atoms created by optical potentials, which can be generated by spatial light modulators[39] or photonic crystals,[40] are also possible approaches to realize the reconfigurable metasurface.

Active TLS Metasurface for Beaming of Spontaneous Emission. A TLS metasurface can also be utilized to control the emission of single photons, which is of importance in quantum information. Existing methods mostly rely on modifying the local optical density of states,[41−43] which involves complex nanostructures. Here we propose to use
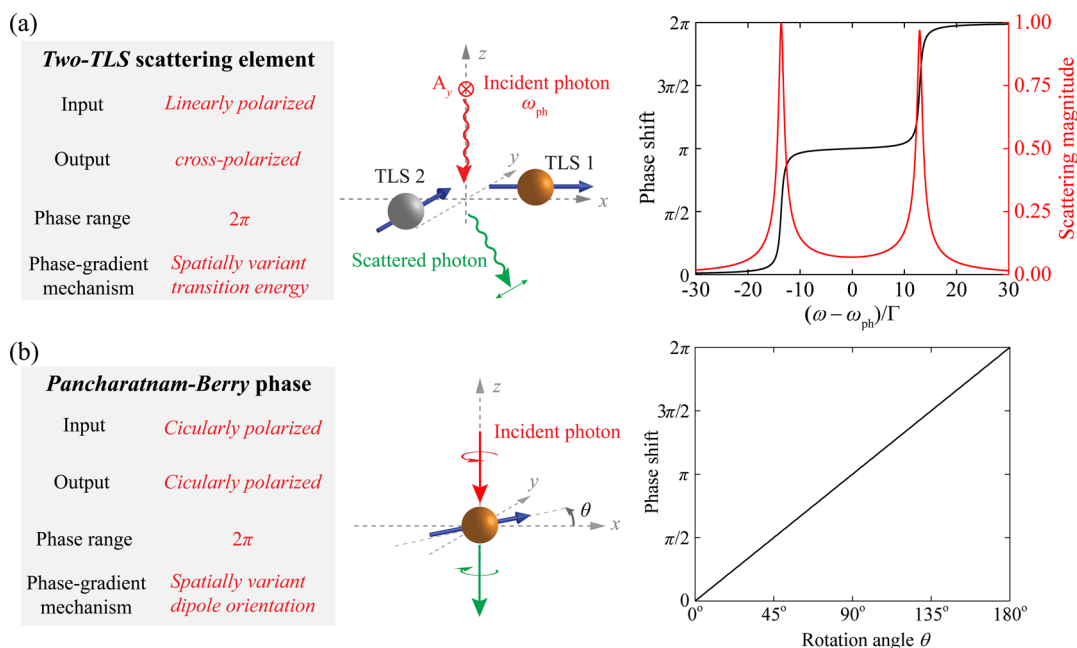
Figure 5. (a) Two-TLS scattering element. A two-TLS scattering element (center panel) consists of two TLSs that have orthogonal dipole moments (blue arrows). The scattering phase (black solid line) and scattering magnitude (red solid line) of scattered photons are plotted in the right panel. The strong near-field interaction between the TLSs creates a subradiant resonance (narrow peak) in addition to the superradiant resonance (broad peak). As a consequence, a 2π phase range is achieved. (b) PB phase created by TLS. When a circularly polarized photon interacts with a TLS, the TLS imparts a geometrical phase to the transmitted photon (center panel). This phase is determined by the orientation of the TLS in the $x-y$ plane. When it rotates 180 deg, a 2π phase range is achieved (right panel).

TLS metasurfaces to realize directional spontaneous emission to a tunable direction. It exploits TLSs' collective interactions to enhance the spatial coherence of the spontaneous emission. Reminiscent of the super- and subradiant effects,[36] the collective interaction in TLS metasurfaces, however, can be engineered with complex phase configuration to allow unprecedented control of spontaneous emission.

To investigate the spontaneous emission in a metasurface, we solve the time-dependent Schrodinger equation to obtain the temporal evolution of the wave function when the initial condition of the metasurface is set to have one TLS in the excited state and no incident photons. To make the calculation feasible on our limited computing facility, we study the case of two-dimensional space, which could be realized by guided waves in planar structure.[44] The working principle is the same in three dimensions.

A single excited TLS in free space emits with a dipole radiation profile (Figure 4a). The same TLS in a metasurface (Figure 4b), however, emits very differently, as shown in Figure 4b. Only one TLS, marked by gold color, is in the excited state, and all other TLSs of the metasurface are in the ground state (Figure 4b). TLSs have different transition energies, configured to scatter photons with different phases (more details in Section 6, Supporting Information). When the other TLSs are partially excited by the spontaneous emission from the initially excited TLS, the spontaneous emission will become quite directional (Figure 4b). To confirm such a prediction, we plot the snapshots of wave functions of the emitted photon at $t = 3\tau$ for a single excited TLS in free space (Figure 4c) and in the metasurface (Figure 4d). A strong directional spatial field is achieved. All TLSs in the metasurface are partially excited through far-field radiative interactions and contribute to the interference that helps to steer the emitted single photon. We further integrate the total flux of the probability integrated over

all time to confirm the highly directional emission and plot them as insets in Figure 4c and d. In contrast to the dipolar profile from a single TLS in free space (Figure 4c inset), the spontaneous emission profile of a metasurface is highly directional (Figure 4d inset). More important, this direction can be controlled by the external inputs by tuning the phase gradient of the metasurface.

Realization of 2π Phase Range. In previous sections, we have demonstrated the unique advantages of a TLS metasurface with simple configurations. Although these simple configurations provide a phase range of only π, the proposed metasurfaces still provide unique optical functionalities with observable efficiency, making the TLS metasurface quite feasible in experiments. In this section, we will discuss approaches to realize a phase range of 2π. On the basis of these approaches, we further provide examples of a metasurface with an efficiency of 98.1% and multiband operation in Sections 4 and 5 of the Supporting Information.

A single resonance provides a scattering phase with a π phase range. However, a 2π phase range is required to obtain maximum steering efficiency. This 2π phase range can be realized in TLS metasurfaces by directly applying one of several approaches developed for conventional metasurfaces, including cross-polarized radiation,[1] Pancharatnam–Berry (PB) phase,[9] and the use of simultaneous electric and magnetic resonances.[4] In this section, we will discuss the strategies to realize a 2π phase range by using multiple TLSs and the PB phase.

Figure 5a shows a composite scattering element consisting of two TLSs that can create a 2π phase range. The two TLSs have the same transition frequency ω_{TLS} but different orientations of the transition dipole moment. The dipole moment of the first TLS (golden sphere) is along the x-axis, and that of the second TLS (gray sphere) is along the y-axis. They are separated by a

spacing of $0.05\lambda_{ph}$, where λ_{ph} is the wavelength of the incident single photons.

At such small spacing, there exists a strong optical near-field interaction between the two TLSs, leading to the cooperative Lamb shift. The strength of the near-field interaction is given by

$$\Omega_{12} = -\frac{3}{4}\Gamma(\hat{x}\cdot\hat{r}_{12})\cdot(\hat{y}\cdot\hat{r}_{12}) \times \left(\frac{\sin k_0 r_{12}}{(k_0 r_{12})} - 3\frac{\sin k_0 r_{12}}{(k_0 r_{12})^2} \right.$$
$$\left. + 3\frac{\cos k_0 r_{12}}{(k_0 r_{12})^3} \right) \tag{2}$$

Here r_{12} and $\hat{r}_{12}$ are the distance and unit vector between the TLSs. The strong near-field interaction creates two resonances: the subradiant and the superradiant modes. Each resonance provides a π phase range as shown in Figure 5a, which shows the scattering phase shift (black solid line) and the scattering amplitude (red solid line) of the cross-polarized scattered photons.

Besides the phase range of 2π, the scattering amplitude also is very important to realize more advance optical functionalities. In conventional metasurfaces, the scattering elements are carefully chosen to have the same scattering amplitude.[1] Such design constraints unfavorably limit the performance of the metasurface. In great contrast, our two-TLS scattering element inherently overcomes the requirement of uniform scattering amplitude. We provide such an example of a two-TLS metasurface with a steering efficiency of 98.1% in Section 4 of the Supporting Information. Multiband operation based on such a metasurface is also demonstrated in Section 5 of the Supporting Information.

Another way to realize a 2π phase range is using a PB phase, which is created when circular polarized light interacts with a TLS (Figure 5b). The TLS functions as a half-wave plate that flips the rotation direction of the circularly polarized light. As show in the center panel in Figure 5b, the TLS has a permanent direction for its dipole moment (blue arrow), which can be found in solid-state TLSs. Its transition energy is detuned from the incident photon's frequency (for example by 2Γ). Depending on the orientation of the TLS in the $x-y$ plane, a geometrical phase from 0 to 2π can be acquired for the transmitted light (right panel in Figure 5b), which is also circularly polarized. A metasurface can be formed by arrays of TLSs with spatially varying orientations.

The potential of TLS metasurfaces goes far beyond the control and the generation of single photons. When illuminated with multiphoton states, TLS metasurfaces can exhibit new dynamics and phenomena that are completely absent in conventional metasurfaces. The most significant is the strong photon−photon interactions induced by the Fermionic excitation of the TLS. Such interactions could make the TLS metasurface an effective antenna to receive, transmit, and create entangled photons, leading to possible applications in quantum information networks. Because of the strong photon−photon interaction and its tunability through external inputs, TLS metasurfaces could also become a versatile platform to study the photonic analogue of many-body physics.

CONCLUSION

In conclusion, we propose to use electronic transition in quantum emitters as a new platform to construct optical metasurfaces. The resonant scattering of electronic transition offers very similar control of single photons as optical resonators. As the building block of metasurfaces, quantum emitters can be extremely compact, nearly lossless, and readily tunable. All these features are not easily achievable in metallic metasurfaces. We also develop a fully quantum mechanical scattering simulator, which is necessary to capture all of the relevant physics of quantum metasurfaces.

ASSOCIATED CONTENT

Ⓢ Supporting Information

The Supporting Information is available free of charge on the ACS Publications website at DOI: 10.1021/acsphotonics.7b00219.

> Detailed description of quantum scattering theory; creating phase gradient by multiple-beam interference; effects of random distributions and densities; example of a high-efficiency metasurface; multiple-band operation of metasurfaces; phase gradient for steering spontaneous emission (PDF)

AUTHOR INFORMATION

Corresponding Author
*E-mail (Z. Yu): zyu54@wisc.edu.
ORCID Ⓘ
Ming Zhou: 0000-0003-2368-8883
Notes
The authors declare no competing financial interest.

ACKNOWLEDGMENTS

REFERENCES

(1) Yu, N.; Genevet, P.; Kats, M. A.; Aieta, F.; Tetienne, J.-P.; Capasso, F.; Gaburro, Z. Light Propagation with Phase Discontinuities: Generalized Laws of Reflection and Refraction. *Science* **2011**, *334*, 333−337.

(2) Zhao, Y.; Alù, A. Manipulating Light Polarization with Ultrathin Plasmonic Metasurfaces. *Phys. Rev. B: Condens. Matter Mater. Phys.* **2011**, *84*, 205428.

(3) Aieta, F.; Genevet, P.; Kats, M. A.; Yu, N.; Blanchard, R.; Gaburro, Z.; Capasso, F. Aberration-Free Ultrathin Flat Lenses and Axicons at Telecom Wavelengths Based on Plasmonic Metasurfaces. *Nano Lett.* **2012**, *12*, 4932−4936.

(4) Sun, S.; Yang, K.-Y.; Wang, C.-M.; Juan, T.-K.; Chen, W. T.; Liao, C. Y.; He, Q.; Xiao, S.; Kung, W.-T.; Guo, G.-Y.; Zhou, L.; Tsai, D. P. High-Efficiency Broadband Anomalous Reflection by Gradient Meta-Surfaces. *Nano Lett.* **2012**, *12*, 6223−6229.

(5) Ni, X.; Emani, N. K.; Kildishev, A. V.; Boltasseva, A.; Shalaev, V. M. Broadband Light Bending with Plasmonic Nanoantennas. *Science* **2012**, *335*, 427−427.

(6) Yin, X.; Ye, Z.; Rho, J.; Wang, Y.; Zhang, X. Photonic Spin Hall Effect at Metasurfaces. *Science* **2013**, *339*, 1405−1407.

(7) Lee, J.; Tymchenko, M.; Argyropoulos, C.; Chen, P.-Y.; Lu, F.; Demmerle, F.; Boehm, G.; Amann, M.-C.; Alù, A.; Belkin, M. A. Giant Nonlinear Response from Plasmonic Metasurfaces Coupled to Intersubband Transitions. *Nature* **2014**, *511*, 65−69.

(8) Wu, C.; Arju, N.; Kelp, G.; Fan, J. A.; Dominguez, J.; Gonzales, E.; Tutuc, E.; Brener, I.; Shvets, G. Spectrally Selective Chiral Silicon Metasurfaces Based on Infrared Fano Resonances. *Nat. Commun.* **2014**, *5*, 3892.

(9) Lin, D.; Fan, P.; Hasman, E.; Brongersma, M. L. Dielectric Gradient Metasurface Optical Elements. *Science* **2014**, *345*, 298−302.

(10) Zheng, G.; Mühlenbernd, H.; Kenney, M.; Li, G.; Zentgraf, T.; Zhang, S. Metasurface Holograms Reaching 80% Efficiency. *Nat. Nanotechnol.* **2015**, *10*, 308−312.

(11) Ni, X.; Wong, Z. J.; Mrejen, M.; Wang, Y.; Zhang, X. An Ultrathin Invisibility Skin Cloak for Visible Light. *Science* **2015**, *349*, 1310−1314.

(12) Hsu, L. Y.; Lepetit, T.; Kante, B. EXTREMELY THIN DIELECTRIC METASURFACE FOR CARPET CLOAKING. *Prog. Electromagn. Res.* **2015**, *152*, 33−40.

(13) Decker, M.; Staude, I.; Falkner, M.; Dominguez, J.; Neshev, D. N.; Brener, I.; Pertsch, T.; Kivshar, Y. S. High-Efficiency Dielectric Huygens' Surfaces. *Adv. Opt. Mater.* **2015**, *3*, 813−820.

(14) Maguid, E.; Yulevich, I.; Veksler, D.; Kleiner, V.; Brongersma, M. L.; Hasman, E. Photonic Spin-Controlled Multifunctional Shared-Aperture Antenna Array. *Science* **2016**, aaf3417.

(15) Falcone, F.; Lopetegi, T.; Laso, M. A. G.; Baena, J. D.; Bonache, J.; Beruete, M.; Marqués, R.; Martín, F.; Sorolla, M. Babinet Principle Applied to the Design of Metasurfaces and Metamaterials. *Phys. Rev. Lett.* **2004**, *93*, 197401.

(16) Holloway, C. L.; Kuester, E. F.; Gordon, J. A.; O'Hara, J.; Booth, J.; Smith, D. R. An Overview of the Theory and Applications of Metasurfaces: The Two-Dimensional Equivalents of Metamaterials. *IEEE Antennas Propag. Mag.* **2012**, *54*, 10−35.

(17) Cao, L.; White, J. S.; Park, J.-S.; Schuller, J. A.; Clemens, B. M.; Brongersma, M. L. Engineering Light Absorption in Semiconductor Nanowire Devices. *Nat. Mater.* **2009**, *8*, 643−647.

(18) Zrenner, A.; Beham, E.; Stufler, S.; Findeis, F.; Bichler, M.; Abstreiter, G. Coherent Properties of a Two-Level System Based on a Quantum-Dot Photodiode. *Nature* **2002**, *418*, 612−614.

(19) Aharonovich, I.; Castelletto, S.; Simpson, D. A.; Stacey, A.; McCallum, J.; Greentree, A. D.; Prawer, S. Two-Level Ultrabright Single Photon Emission from Diamond Nanocrystals. *Nano Lett.* **2009**, *9*, 3191−3195.

(20) Astafiev, O.; Zagoskin, A. M.; Abdumalikov, A. A.; Pashkin, Y. A.; Yamamoto, T.; Inomata, K.; Nakamura, Y.; Tsai, J. S. Resonance Fluorescence of a Single Artificial Atom. *Science* **2010**, *327*, 840−843.

(21) Boller, K.-J.; Imamolu, A.; Harris, S. E. Observation of Electromagnetically Induced Transparency. *Phys. Rev. Lett.* **1991**, *66*, 2593−2596.

(22) Tamarat, P.; Gaebel, T.; Rabeau, J. R.; Khan, M.; Greentree, A. D.; Wilson, H.; Hollenberg, L. C. L.; Prawer, S.; Hemmer, P.; Jelezko, F.; Wrachtrup, J. Stark Shift Control of Single Optical Centers in Diamond. *Phys. Rev. Lett.* **2006**, *97*, 083002.

(23) Trepanier, M.; Zhang, D.; Mukhanov, O.; Anlage, S. M. Realization and Modeling of Metamaterials Made of Rf Super-conducting Quantum-Interference Devices. *Phys. Rev. X* **2013**, *3*, 041029.

(24) Yao, Y.; Shankar, R.; Kats, M. A.; Song, Y.; Kong, J.; Loncar, M.; Capasso, F. Electrically Tunable Metasurface Perfect Absorbers for Ultrathin Mid-Infrared Optical Modulators. *Nano Lett.* **2014**, *14*, 6526−6532.

(25) Fan, Y.; Shen, N.-H.; Koschny, T.; Soukoulis, C. M. Tunable Terahertz Meta-Surface with Graphene Cut-Wires. *ACS Photonics* **2015**, *2*, 151−156.

(26) Huang, Y.-W.; Lee, H. W. H.; Sokhoyan, R.; Pala, R. A.; Thyagarajan, K.; Han, S.; Tsai, D. P.; Atwater, H. A. Gate-Tunable Conducting Oxide Metasurfaces. *Nano Lett.* **2016**, *16*, 5319.

(27) Wang, Q.; Rogers, E. T. F.; Gholipour, B.; Wang, C.-M.; Yuan, G.; Teng, J.; Zheludev, N. I. Optically Reconfigurable Metasurfaces and Photonic Devices Based on Phase Change Materials. *Nat. Photonics* **2016**, *10*, 60−65.

(28) Michler, P.; Kiraz, A.; Becher, C.; Schoenfeld, W. V.; Petroff, P. M.; Zhang, L.; Hu, E.; Imamoglu, A. A Quantum Dot Single-Photon Turnstile Device. *Science* **2000**, *290*, 2282−2285.

(29) Ficek, Z.; Swain, S. *Quantum Interference and Coherence: Theory and Experiments*; Springer Science & Business Media, 2005.

(30) Bohren, C. F.; Huffman, D. R. *Absorption and Scattering of Light by Small Particles*; Wiley-VCH, 1983.

(31) Aieta, F.; Kats, M. A.; Genevet, P.; Capasso, F. Multiwavelength Achromatic Metasurfaces by Dispersive Phase Compensation. *Science* **2015**, *347*, 1342−1345.

(32) Dung, H. T.; Knöll, L.; Welsch, D.-G. Resonant Dipole-Dipole Interaction in the Presence of Dispersing and Absorbing Surroundings. *Phys. Rev. A: At., Mol., Opt. Phys.* **2002**, *66*, 063810.

(33) Shen, J.-T.; Fan, S. Coherent Single Photon Transport in a One-Dimensional Waveguide Coupled with Superconducting Quantum Bits. *Phys. Rev. Lett.* **2005**, *95*, 213001.

(34) Liu, J.; Zhou, M.; Yu, Z. Quantum Scattering Theory of a Single-Photon Fock State in Three-Dimensional Spaces. *Opt. Lett.* **2016**, *41*, 4166−4169.

(35) Li, Y.; Xiao, M. Electromagnetically Induced Transparency in a Three-Level Λ-Type System in Rubidium Atoms. *Phys. Rev. A: At., Mol., Opt. Phys.* **1995**, *51*, R2703.

(36) Dicke, R. H. Coherence in Spontaneous Radiation Processes. *Phys. Rev.* **1954**, *93*, 99−110.

(37) Brown, A. W.; Xiao, M. All-Optical Switching and Routing Based on an Electromagnetically Induced Absorption Grating. *Opt. Lett.* **2005**, *30*, 699.

(38) Juska, G.; Dimastrodonato, V.; Mereni, L. O.; Gocalinska, A.; Pelucchi, E. Towards Quantum-Dot Arrays of Entangled Photon Emitters. *Nat. Photonics* **2013**, *7*, 527−531.

(39) Nogrette, F. Single-Atom Trapping in Holographic 2D Arrays of Microtraps with Arbitrary Geometries. *Phys. Rev. X* **2014**, *4*, 4.

(40) González-Tudela, A.; Hung, C.-L.; Chang, D. E.; Cirac, J. I.; Kimble, H. J. Subwavelength Vacuum Lattices and Atom−atom Interactions in Two-Dimensional Photonic Crystals. *Nat. Photonics* **2015**, *9*, 320−325.

(41) Noda, S.; Fujita, M.; Asano, T. Spontaneous-Emission Control by Photonic Crystals and Nanocavities. *Nat. Photonics* **2007**, *1*, 449−458.

(42) Belacel, C.; Habert, B.; Bigourdan, F.; Marquier, F.; Hugonin, J.-P.; Michaelis de Vasconcellos, S.; Lafosse, X.; Coolen, L.; Schwob, C.; Javaux, C.; Dubertret, B.; Greffet, J.-J.; Senellart, P.; Maitre, A. Controlling Spontaneous Emission with Plasmonic Optical Patch Antennas. *Nano Lett.* **2013**, *13*, 1516−1521.

(43) Newman, W. D.; Cortes, C. L.; Jacob, Z. Enhanced and Directional Single-Photon Emission in Hyperbolic Metamaterials. *J. Opt. Soc. Am. B* **2013**, *30*, 766−775.

(44) Fan, S.; Joannopoulos, J. D. Analysis of Guided Resonances in Photonic Crystal Slabs. *Phys. Rev. B: Condens. Matter Mater. Phys.* **2002**, *65*, 235112.